

# Earthquake source mechanisms from body-waveform inversion and intraplate tectonics in the northern Indian Ocean

Eric A. Bergman and Sean C. Solomon

*Department of Earth, Atmospheric, and Planetary Sciences, Massachusetts Institute of Technology, Cambridge, MA 02139 (U.S.A.)*

(Received December 20, 1984; revision accepted March 6, 1985)

Bergman, E.A. and Solomon, S.C., 1985. Earthquake source mechanisms from body-waveform inversion and intraplate tectonics in the northern Indian Ocean. *Earth Planet. Inter.*, 40: 1–23.

Double-couple point-source parameters for 11 of the largest intraplate earthquakes in the northern Indian Ocean during the last 20 y were determined from a formal inversion of long-period P and SH waveforms. Nine of the events have centroid depths at least 17 km below the seafloor, well into the upper mantle; two have centroid depths as great as 39 km. Using the source mechanisms of these earthquakes, we distinguish two major intraplate tectonic provinces in the northern Indian Ocean. To the west of the Ninetyeast Ridge, in the southern Bay of Bengal, intraplate earthquakes have thrust-faulting mechanisms with P axes oriented N–S. The centroid depths of these earthquakes range from 27 to 39 km below the seafloor. Lithospheric shortening in this region is thus accomplished by thrust faulting in the strong core of the oceanic upper mantle, while other geophysical evidence suggests that shallow sedimentary and crustal layers apparently deform predominantly by folding. In the immediate vicinity of the Ninetyeast Ridge, earthquakes display strike-slip mechanisms with left-lateral motion on planes parallel to the ridge. This type of faulting occurs from at least 10°S to the northern end of the Ninetyeast Ridge near 10°N, where the ridge meets the Sunda Arc. Seismic activity diminishes to the east of the Ninetyeast Ridge, but is also characterized by strike-slip faulting. Despite these variations in deformational style, the inferred orientation of greatest compressive stress in the northern Indian Ocean displays a consistent long-wavelength pattern over a large portion of the Indian plate, varying smoothly from nearly N–S in the Bay of Bengal to NW–SE in the northeastern Indian Ocean. This plate-wide stress pattern and the high level of intraplate seismicity in the northern Indian Ocean are likely the results of substantial resistance, along the Himalayan continental collision zone, to the continued northward motion of the western portion of the Indian plate. Oceanic intraplate earthquakes in other regions, where the level of deviatoric stress associated with the long-wavelength part of the stress field is likely to be smaller, need not be comparably reliable indicators of the plate-wide stress field.

## 1. Introduction

The northern Indian Ocean has been the most seismically active oceanic intraplate region in this century. Gutenberg and Richter (1954) were the first to comment on the frequent occurrence in the northern Indian Ocean of earthquakes with little apparent connection to other prominent seismic belts. They also noted the association of many oceanic intraplate earthquakes with the Ninetyeast Ridge. Stein and Okal (1978) observed that the Ninetyeast Ridge has been approximately as seismically active as Southern California during

this century. The young oceanic lithosphere of the Indian plate also experiences unusually high levels of intraplate seismicity (Stein, 1978; Bergman and Solomon, 1984; Bergman et al., 1984). Additional studies of Indian Ocean seismicity have been reported by Stover (1966) and Rothe (1969). Sykes (1970) interpreted the seismicity pattern of the northern Indian Ocean for the years 1950–1966 as evidence for an incipient island arc complex between Sri Lanka and Australia. The distribution of epicenters since 1964, however, is characterized by a trend oriented more nearly N–S than NW–SE, and no other evidence has been found to support

the nascent island arc hypothesis (Stein and Okal, 1978; Weissel et al., 1980).

From a study of the seismicity in the Ninetyeast Ridge area and the source mechanisms of several of the larger earthquakes in the region, Stein and Okal (1978) concluded that the northern part of the Ninetyeast Ridge is an active seismic zone along which both strike-slip and some vertical motion occur. They suggested that the Ninetyeast Ridge is the site of at least partial decoupling of the western and eastern halves of the Indian plate, caused by resistance to northward motion of the western part of the plate along the zone of continental collision with Asia.

Evidence for a different style of deformation in the Indian plate to the west of the Ninetyeast Ridge has been reported by Weissel et al. (1980) and Geller et al. (1983). Faulting and deformational structures in the oceanic crust and sediments, zones of anomalously high heat flow, and large earthquakes in this area all suggest significant ongoing intraplate deformation characterized by compression and shortening in a N-S direction.

To understand better the nature of large-scale internal deformation in oceanic lithosphere of the Indian plate, we conducted detailed source studies of 11 intraplate earthquakes in the northern Indian Ocean. Focal mechanisms, seismic moments, source time functions, and centroid depths were obtained by an inversion of long-period P and SH waveforms. The frequent occurrence of large earthquakes in this area also allowed us to examine the coherency of the long-wavelength intraplate stress field and the reliability of principal stress orientations inferred from the focal mechanisms of earthquakes in oceanic lithosphere.

## 2. Tectonic setting

An understanding of the intraplate seismicity of the Indian plate must be set in the context of the tectonic history of the region. The evolution of oceanic lithosphere in the Indian Ocean has been the subject of numerous studies; data obtained by the Deep-Sea Drilling Program have led to general agreement on the major elements of a broad model

(Veevers, 1977). According to the syntheses of Johnson et al. (1976) and Curray et al. (1982), the initial breakup of Gondwanaland occurred about 125 Ma ago, when the Indian plate separated from Antarctica–Australia along an axis parallel to the present southeast coast of India. Creation of oceanic lithosphere at this spreading axis continued until about 90 Ma ago. At some time between 110 and 80 Ma ago, a spreading ridge system developed between India and Antarctica, which had been separated previously by a transform boundary. Slow spreading between Antarctica and Australia may have begun at this time also (Mutter and Cande, 1983). The resulting motion of the Indian plate was approximately N–S, parallel to a long oceanic transform fault on the eastern side of the Ninetyeast Ridge. The en echelon pattern in the bathymetry of the northern part of the Ninetyeast Ridge (presently from about 5°S to at least 10°N) developed at this time when the SW–NE trending ridge axis was reorganized into a series of short E–W trending ridge segments, offset in a left-lateral sense by N–S trending fracture zones. The Indian plate moved rapidly north at about 100 mm y<sup>-1</sup> until about 53 Ma ago, when the Indian continent made initial contact with Asia. At about 46 Ma ago, spreading ceased in the northwestern Wharton Basin, east of the Ninetyeast Ridge (Liu et al., 1983). The onset of spreading on the present Southeast Indian Ridge inaugurated the current stage in the tectonic evolution of the Indian Ocean, in which the former Indian and Australian plates have moved approximately as a single plate. The Ninetyeast Ridge marks a dramatic transition in the tectonic style of the northern boundary of this plate. The Australian half of the plate is being subducted along the Sunda Arc to the east. To the west of the Ninetyeast Ridge the continental collision between India and Asia has continued, perhaps in several stages, as the Indian continent collided first with an island arc and eventually with the Asian continent. The present distribution of major bathymetric and tectonic features in the northern Indian Ocean is shown in Fig. 1.

The Ninetyeast Ridge plays a prominent role in the tectonic framework of the northern Indian Ocean. The ridge extends over 5000 km, from

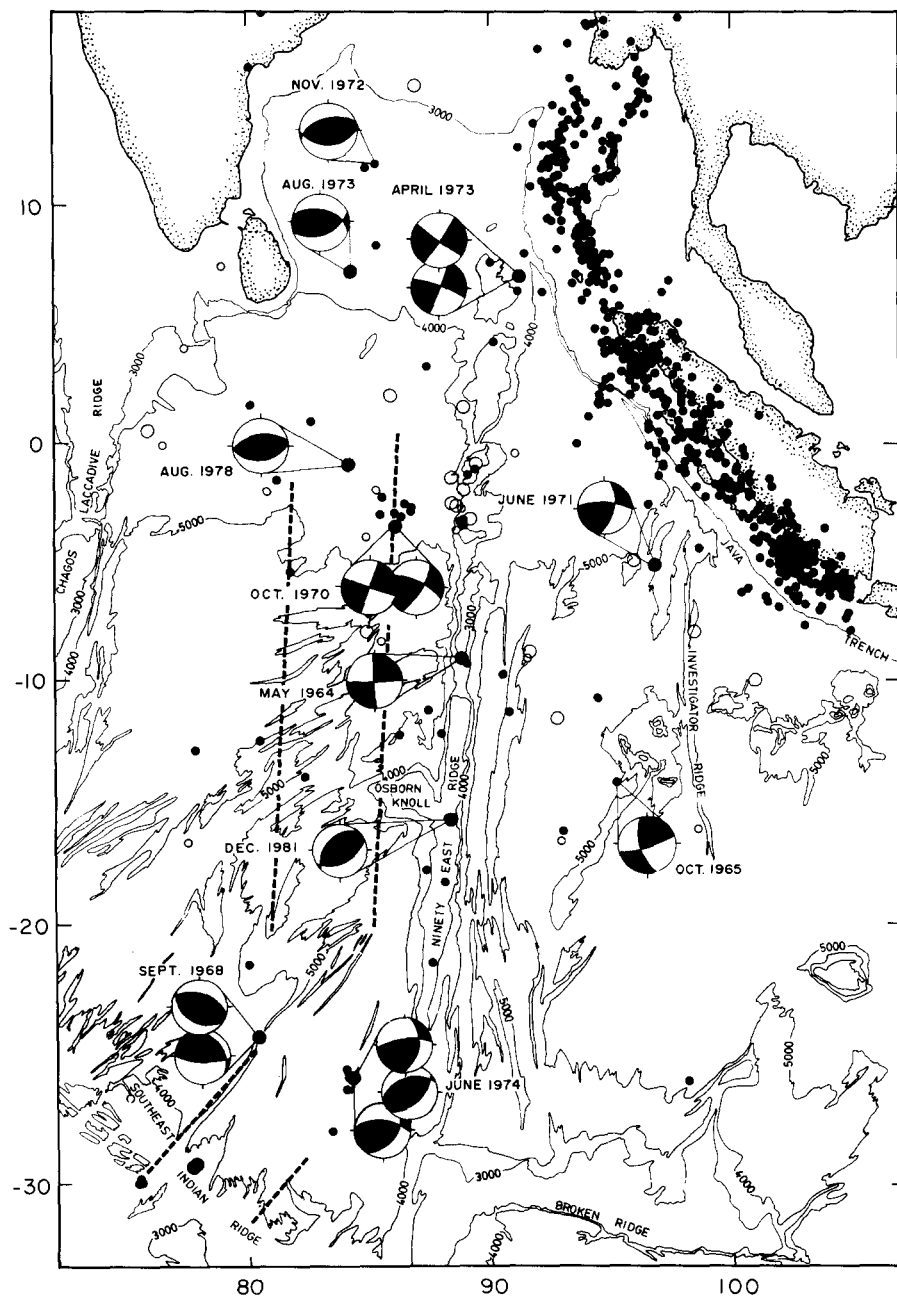


Fig. 1. Seismicity and bathymetry of the study area in the northern Indian Ocean. Bathymetric contours (3000, 4000 and 5000 m) are from Laughton (1975) and Fisher et al. (1982). Several fracture zones west of the Ninetyeast Ridge identified by Sclater and Fisher (1974) are indicated by dashed lines. Open circles indicate epicenters of earthquakes which occurred between 1906 and 1963, with larger symbols for events with  $M$  or  $M_s \geq 6.0$ . Solid circles indicate epicenters of earthquakes since 1964, with larger symbols for events with  $m_b \geq 5.4$ . Focal mechanisms were determined by body-waveform inversion and are summarized in Table I. Four events were modeled with two (or three, in the case of the June 25, 1974 earthquake) point sources, as described in the text.

about 31°S to at least 17°N (Fig. 1), but north of 10°N it is buried beneath sediments of the Bengal Deep-Sea Fan (Curry et al., 1982). The ridge ranges in width between 150 and 250 km. North of about 6°S the ridge has a blocky en echelon structure. In contrast, the southern part of the ridge is relatively straight and flat-topped but becomes wider at about 15°S, the latitude of the Osborn Knoll, a prominent bathymetric feature on the western flank of the ridge. Gravity data indicate that the ridge is isostatically compensated, probably by emplacement of relatively less dense material in the upper mantle beneath a fairly normal oceanic crustal layer (Bowin, 1973). Such a structure is also consistent with seismic refraction data (Francis and Raitt, 1967). The Ninetyeast Ridge apparently has always been attached to the Indian plate and has subsided at the same rate as normal oceanic lithosphere (Sclater and Fisher, 1974; Detrick et al., 1977).

Early theories on the origin of the Ninetyeast Ridge have been summarized by Schlich (1982). They range from its being a microcontinent to being an uplifted horst-like feature resulting from compression between the Indian and Australian halves of the plate. There is now general agreement that the bathymetric expression of the Ninetyeast Ridge results from the passage of the Indian plate over a mantle hotspot. Support for a hotspot origin for the Ninetyeast Ridge comes from paleomagnetic data indicating that the ridge was formed at high southern latitudes (Peirce, 1978) and paleontological evidence that it formed at or near sealevel (Luyendyk and Davies, 1974). According to the current model the hotspot lay beneath the Indian continent until about 90 Ma ago. The rapid northward motion of the Indian plate after this time carried the en echelon pattern of former spreading ridge segments of the northern part of the Ninetyeast Ridge over the hotspot, building the bathymetric level up to near sea-level (Curry et al., 1982). The change in morphology of the ridge near the Osborn Knoll corresponds to the location of the hotspot at the time of the initial collision between India and Asia, when the velocity of the Indian plate relative to the hotspot is likely to have decreased (Curry et al., 1982).

### 3. Earthquake source mechanisms

Epicentral data for the 11 earthquakes treated in this study are listed in Table I. During the 20 year period 1964–1983, there have been few if any other intraplate earthquakes in the northern Indian Ocean of a size sufficient for body-waveform modeling. For each earthquake, we determined the best-fitting double-couple point source from an inversion of long-period P and SH waveforms, most of which were recorded at stations of the World-Wide Standard Seismograph Network (WWSSN). A few records from the Global Digital Seismic Network (GDSN) were also used. For one very small and shallow event, we obtained increased resolution of the rupture history through the use of short-period P waveforms. We used the inversion technique of Nabelek (1984); details of the procedure are also discussed in Bergman et al. (1984) and Bergman and Solomon (1984). The inversion yields estimates of the centroid depth, double-couple orientation, seismic moment, and source time function. The orientation of the best-fitting double couple, specified using the convention of Aki and Richards (1980), is determined to within about  $\pm 5^\circ$  in each angular coordinate, and the moment to within about  $\pm 30\%$  at the  $2\sigma$  (95% confidence) level. The formal error ( $2\sigma$ ) in centroid depth is typically  $\pm 0.5$  to 1.0 km, but because of bias introduced by factors not reflected in the *a posteriori* estimate of parameter variance, such as the alignment in time of the synthetic and observed waveforms, the true uncertainty is greater, perhaps  $\pm 2$  km in a typical case. Depth resolution is improved significantly by the use of short-period waveform data. The resolution of all source parameter estimates may be degraded by such factors as poor station distribution, poor signal-to-noise ratio, or source complexity.

Substantial improvements in our understanding of the faulting process have resulted from the recognition that stress is distributed, in general, quite heterogeneously on faults (e.g., Das and Aki, 1977; Ebel and Helmberger, 1982; Rundle et al., 1984). The ability to resolve such details of the earthquake source depends on the completeness with which the data sample the radiation pattern and also on the pass band of the observing instru-

TABLE I

Epicentral data <sup>a</sup> and source parameters for earthquakes in the northern Indian Ocean

Month	Day	Year	Origin time	Lat. °N	Long. °E	$m_b$	$M_s$	$M_0$ <sup>b</sup>	Mechanism <sup>c</sup>	Centroid depth <sup>d</sup>
5	25	64	1944:05.9	-9.08	88.89	5.7	6.0	9.6	177/87/005	17
10	31	65	1724:09.5	-14.22	95.27	5.3	5.4	6.1	165/68/009	24
9	14	68 <sup>e</sup>	0125:18.9	-24.45	80.41	5.4		0.3	291/48/082	3
								0.4	315/23/129	4
10	10	70 <sup>e</sup>	0853:04.5	-3.56	86.19	5.8	6.3	41	019/89/358	27
								21	032/73/021	39
6	26	71	1927:11	-5.18	96.90	5.9	6.4	54	014/67/019	29
11	24	72	1319:14.3	11.67	85.34	5.2	5.2	3.0	254/52/076	27
4	7	73 <sup>e</sup>	0300:59.6	7.00	91.32	5.8	6.6	25	034/84/356	13
								83	020/87/009	6
8	30	73	1950:03.9	7.15	84.33	5.8	5.2	3.7	290/52/118	27
6	25	74 <sup>e</sup>	1722:17.9	-26.02	84.30	6.1	6.6	110	010/50/025	23
								26	047/53/073	18
								11	036/48/041	13
8	3	78	0110:26	-0.93	84.24	5.5	5.5	5.9	261/53/090	39
12	2	81	1901:53.9	-15.76	88.39	5.7	5.5	5.8	222/44/078	23

<sup>a</sup> Source: International Seismological Center (ISC), except for surface wave magnitude  $M_s$  for May 25, 1964 (Stein and Okal, 1978) and October 31, 1965 (Wiens and Stein, 1983).

<sup>b</sup> Seismic moment in units of  $10^{24}$  dyn-cm ( $10^{17}$  N-m).

<sup>c</sup> Focal mechanism (strike, dip, slip, all in degrees) specified with the convention of Aki and Richards (1980).

<sup>d</sup> Relative to the top of the crust (or sediment layer, if used), km.

<sup>e</sup> This event was modeled with more than one point source. See text for further discussion.

ments relative to the scale of the heterogeneities. We significantly improved the fit to the observed waveforms for four of the earthquakes in this study by using a multiple point-source model. For three of the largest earthquakes, the need for a more complex source model (two or three sub-events) was evident in the long-period waveforms; the short-period P waveforms used to improve depth resolution for the smallest earthquake in our data set revealed complexity which could not be resolved with long-period waveform data. In addition to the normal centroid parameters for each subevent, we inverted in these cases for the relative location and time delay of the later sub-events with respect to the first.

Except for several cases (noted below) in which a sediment layer was included, we conducted all inversions with the same source velocity structure: a water layer with depth estimated from bathymetric maps, a single crustal layer of thickness 6 km and P and S-wave velocities of  $\alpha = 6.4$  km s<sup>-1</sup> and  $\beta = 3.7$  km s<sup>-1</sup>, respectively, and a mantle half-space with  $\alpha = 8.1$  km s<sup>-1</sup> and  $\beta = 4.6$  km s<sup>-1</sup>.

Centroid depths are given relative to the top of the crustal layer or to the top of the sediment layer, if one was used.

Departures of the real Earth from our simple source velocity structure undoubtedly introduce some bias into the inversion results, primarily for the centroid depth, the estimate of which is strongly coupled to the vertical travel time from the centroid to the seafloor. The velocity structure of oceanic crust and upper mantle is generally observed to vary only within a rather narrow range, and errors introduced by such variations are unlikely to be significant (compared to the other sources of uncertainty discussed above) for events in "normal" oceanic lithosphere. Several events in this study, however, occurred in areas where the true velocity structure may depart significantly from that assumed for the inversion, and the potential for bias in our results for these events should be noted. The May 25, 1964, April 7, 1973, and December 2, 1981 earthquakes are located on the Ninetyeast Ridge, which may be underlain by a thickened crustal layer or an upper mantle with anomalously

low seismic velocities (Bowin, 1973). In either case, the centroid depths reported here for these events would be biased toward greater values. For example, the best-fitting centroid for the May 1964 event is about 1.5 km shallower if we assume a crustal thickness of 10 km rather than 6 km. A potential for bias in the estimated centroid depth also exists for several earthquakes in the Bay of Bengal because of the extremely thick layer of sediments. Our estimate of the thickness and average velocity of the sedimentary layer in these cases is probably accurate enough to limit any associated bias in centroid depth to 1 km or less. The assumption that these sediments are underlain by normal oceanic crust and upper mantle, however, may be open to question.

The derived focal mechanisms and the comparison of observed and synthetic waveforms are given in a series of figures; P waves and SH waves are shown on separate focal spheres (each with the appropriate radiation pattern) for clarity. The synthetics shown have not been individually rescaled for improved fit. The station codes and geographic locations of all stations used in the inversions may

be found in Poppe et al. (1978). The best-fitting source parameters for the 11 earthquakes are given in Table I, and their focal mechanisms are shown in Fig. 1.

### 3.1. May 25, 1964

The May 25, 1964 earthquake occurred on the northern Ninetyeast Ridge, at the southern end of the portion of the ridge which has been most seismically active in this century (Stein and Okal, 1978). Station coverage for P waveforms is limited basically to the Northern Hemisphere (Fig. 2), but we obtained excellent SH wave records over a wide range of azimuths, including four near-nodal stations (HKC, ADE, HLW, and SHI). Consequently, the best-fitting double couple (177/87/5) is well constrained. This mechanism is quite similar to that found by Banghar and Sykes (1969) from first motion polarities. The seismic moment determined in the inversion,  $9.6 \times 10^{24}$  dyn-cm, agrees well with the value of  $1.1 \times 10^{25}$  dyn-cm estimated from surface waves by Stein and Okal (1978). The centroid depth of 17 km is identical to

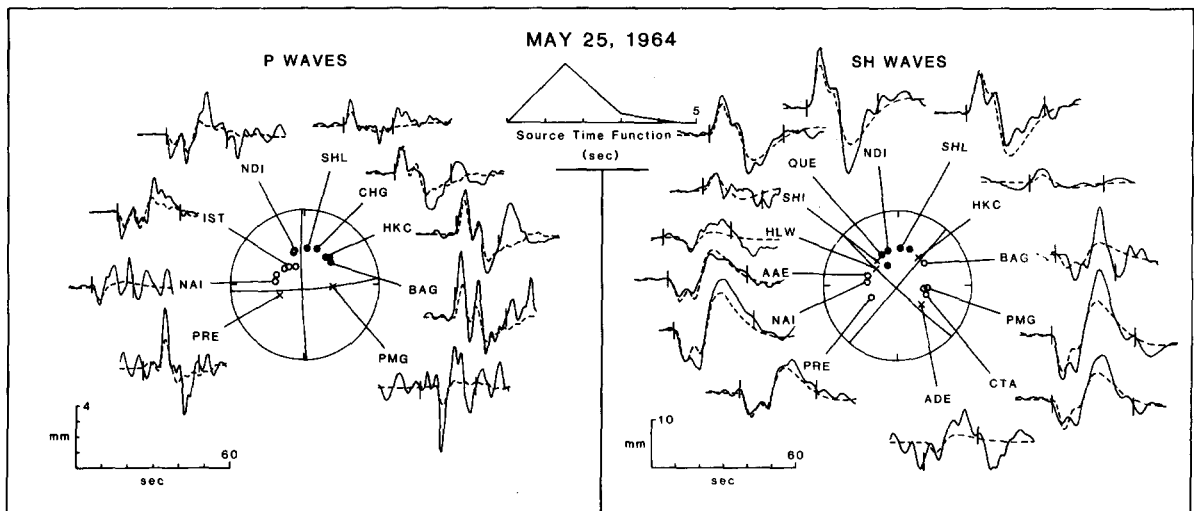


Fig. 2. Comparison of observed long-period P and SH waves (solid lines) from the May 25, 1964 earthquake with synthetic waveforms (dashed lines) generated for the best-fitting point source mechanism found in the body-waveform inversion. P and SH radiation patterns are shown on the lower focal hemisphere (equal area projection). The source time function obtained from the inversion is also shown. All amplitudes are normalized to an instrument magnification of 3000; the amplitude scales correspond to the waveforms that would be observed on an original seismogram from such an instrument. The two vertical lines delimit the portion of each time series used in the inversion. Symbols for both types of waves are: open circle—dilatation, closed circle—compression, cross—emergent arrival. For SH waves, compression corresponds to positive motion as defined by Aki and Richards (1980). First motions read from long-period seismograms but not used in the inversion are also plotted.

that estimated by Wiens and Stein (1983) from matching P waveforms. The SH waves are matched well with a simple triangular source time function about 3 s in duration. A somewhat more complicated source is suggested by some of the P waveforms, but we found no multiple source model which yielded a significant improvement in overall fit as compared to the single point-source model shown in Fig. 2.

### 3.2. October 31, 1965

The earthquake on October 31, 1965 occurred southwest of the Cocos-Keeling Seamount in the northeast Indian Ocean. This earthquake was well recorded, and station coverage for both P and SH waves is very good, considering the remoteness of the epicenter. The polarity of the horizontal component instruments at PRE was found to be reversed; the observed SH waveform has been correspondingly corrected. The observed P and SH waves are exceptionally well matched by the synthetic waveforms (Fig. 3). The mechanism is characterized by strike-slip faulting, with a P axis oriented NW-SE (165/68/9). The seismic moment is  $6.1 \times 10^{24}$  dyn-cm, and the centroid depth is 24 km below the seafloor. Our mechanism is

quite similar to that obtained by Wiens and Stein (1983) from first motions and P wave modeling (167/77/3). They also estimated the depth to be 24 km.

### 3.3. September 14, 1968

Sykes and Sbar (1974) characterized the September 14, 1968 earthquake as a thrust-faulting event, but they were unable to determine the strike of the nodal planes from first motion polarities alone. The epicenter lies in an area where major fracture zone trends change direction from NE-SW to N-S (Fig. 1); the lithosphere may locally display a relatively complex pattern of faulting. This small event yielded clear short-period records at many stations, but we found only four high-gain stations at which the long-period P waveforms were recorded clearly enough to permit an inversion. SH waveforms were obtained for seven stations, but the signal-to-noise ratio is rather low and, as with the P waves, the azimuthal distribution of stations is poor. The horizontal component instruments at PRE were found to have reversed polarity; the SH waveform was corrected prior to the inversion. Using these long-period data, the inversion converged to a solution char-

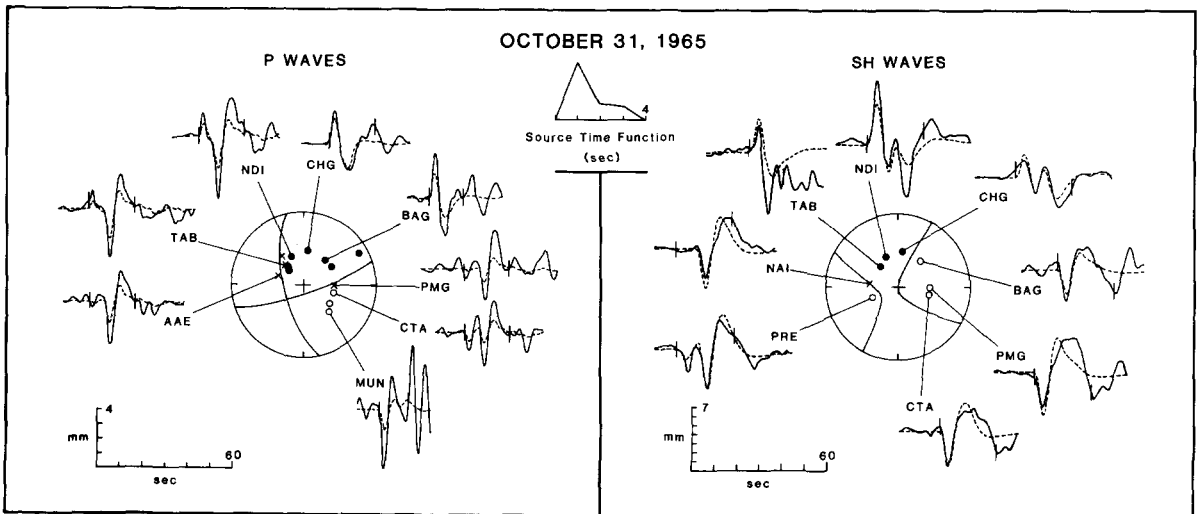


Fig. 3. Comparison of observed P and SH waves from the October 31, 1965 earthquake with synthetic waveforms generated for the best-fitting point source mechanism found in the body-waveform inversion. See Fig. 2 for further explanation.

acterized by nearly pure thrust faulting with a P axis oriented NNE (296/46/94), with a seismic moment of  $6.4 \times 10^{23}$  dyn-cm and a centroid depth of 4 km.

Because of the poor station distribution and low signal-to-noise ratio of the long-period waveform data for this earthquake, the uncertainties in the derived source parameters are larger than normal. We attempted to improve the resolution of these parameters, particularly the centroid depth, by repeating the inversion with the addition of short-period P waveforms from three well-distributed stations: PRE, CHG, and CTA (Fig. 4). These waveforms are very representative of the full set of short-period records. The seismograms were digitized at an interval of 0.1 s rather than the 0.5 s used for long-period waveforms, but in all other respects the short period waveforms were processed in a manner identical to that used for the long-period data. However, there is one significant complication in using short-period P waves in the inversion. Compared to the typical value of 1 s assumed for the attenuation parameter  $t^*$  for long-period P waves, the value of  $t^*$  at shorter

periods is much more variable, with reported values at a frequency of 1 Hz between 0.5 and 1.3 s, depending on the propagation path (Cormier, 1982; Der et al., 1982). Synthetic short-period waveforms are very sensitive to  $t^*$ ; unless amplitude information is ignored in the inversion (Nabelek, 1984), an independent estimate of this parameter must be made to prevent instabilities. We estimated  $t^*$  for the propagation paths to the three short-period P wave stations by forward modeling before performing the final inversion. A value of 0.5 s reproduces the high frequencies and amplitudes of the observed waveforms at PRE and CTA, but a good match to the P waveform at CHG requires higher attenuation (0.8 s).

The addition of a small number of short-period waveforms in the inversion not only led to a significant improvement in depth resolution, but also revealed complexity in the source process of this small earthquake which is completely invisible to long-period instruments. The observed short-period P waveforms at PRE and CTA (and all other stations to the east or west) are quite similar in shape, and a single point source solution which

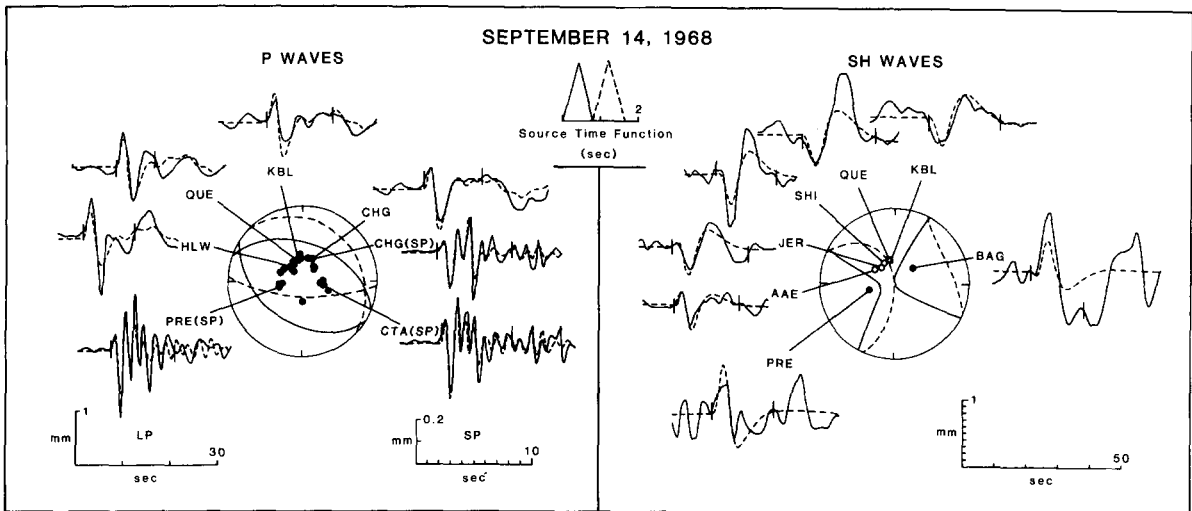


Fig. 4. Comparison of observed P and SH waves from the September 14, 1968 earthquake with synthetic waveforms generated with a model consisting of two point sources, the parameters of which were found in the body-waveform inversion. Dashed lines indicate the source time function and focal mechanism of the second subevent. The delay between the centroidal times of the subevents is shown; the apparent delay at any station depends on the angle between the line joining the subevents and the raypath. Long- and short-period P waveforms are plotted with different time-amplitude scales. See the text and Fig. 2 for further explanation.

fits them as well as the long-period waveforms is readily obtainable. All the short period waveforms recorded to the north (represented here by CHG), however, have a distinctly different shape, and no single-source solution can match simultaneously all the short and long-period waveforms. Inversion of short-period waveforms is much less robust than when long-period data alone are used, and many different single-source starting models were tried before we concluded that a double point source model is required by the data.

We constrained the source time functions of the two subevents in the multiple source model to be triangular in shape and 0.8 s in duration, but the relative location and time delay of the second subevent with respect to the first were included as free parameters in the inversion. An excellent fit to all the observed waveforms was obtained with a source model in which the second subevent is located 7 km north of the first and delayed by 0.8 s. This offset to the north accounts for the differences between the short-period P waves observed to the north and those recorded to the east and west. The focal mechanism of the first subevent (291/48/82) is very similar to the long-period solution mentioned above, while the second

subevent (315/23/129) is characterized by thrust or reverse faulting with one steep and one shallow nodal plane (Fig. 4). The resolution of these focal mechanisms is rather poor, however, with standard errors ( $2\sigma$ ) of between  $5^\circ$  and  $10^\circ$  for the strike and slip angles of the two subevents and somewhat smaller uncertainties for the dip angles. The seismic moments of the two subevents are  $3.0 \times 10^{23}$  and  $4.0 \times 10^{23}$  dyn-cm, respectively. The centroid depth of the first subevent is 3.2 km and that of the second is 3.6 km, with a standard error ( $2\sigma$ ) of less than 100 m. With the short-period data, the depth resolution is about an order of magnitude better than that obtained when long-period data alone are used.

#### 3.4. October 10, 1970

On the basis of P-wave first motions and S-wave polarizations, Fitch (1972) determined a nearly pure strike-slip mechanism (126/83/164) for the earthquake of October 10, 1970. From magnetic anomaly identifications, Sclater and Fisher (1974) proposed that a large N-S trending fracture zone passes through the epicentral region of this event (Fig. 1). Curray et al. (1982) questioned this in-

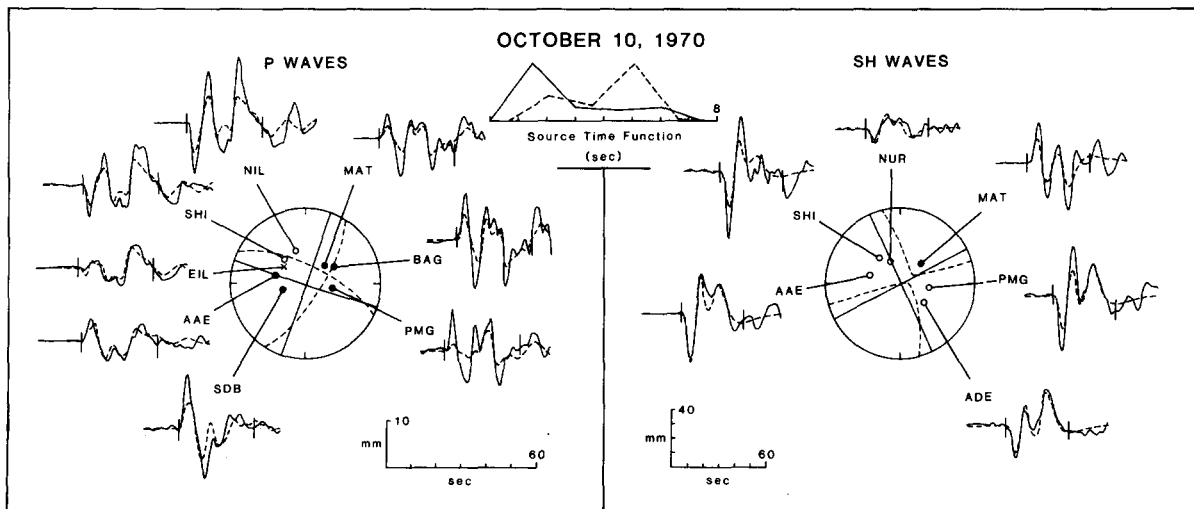


Fig. 5. Comparison of observed P and SH waves from the October 10, 1970 earthquake with synthetic waveforms generated with a model consisting of two point sources, the parameters of which were found in the body-waveform inversion. The dashed lines in the source time function and focal mechanisms represent the second subevent. The delay between the centroidal times of the subevents is shown; the apparent delay at any station depends on the angle between the line joining the subevents and the raypath. See Fig. 2 and the text for further explanation.

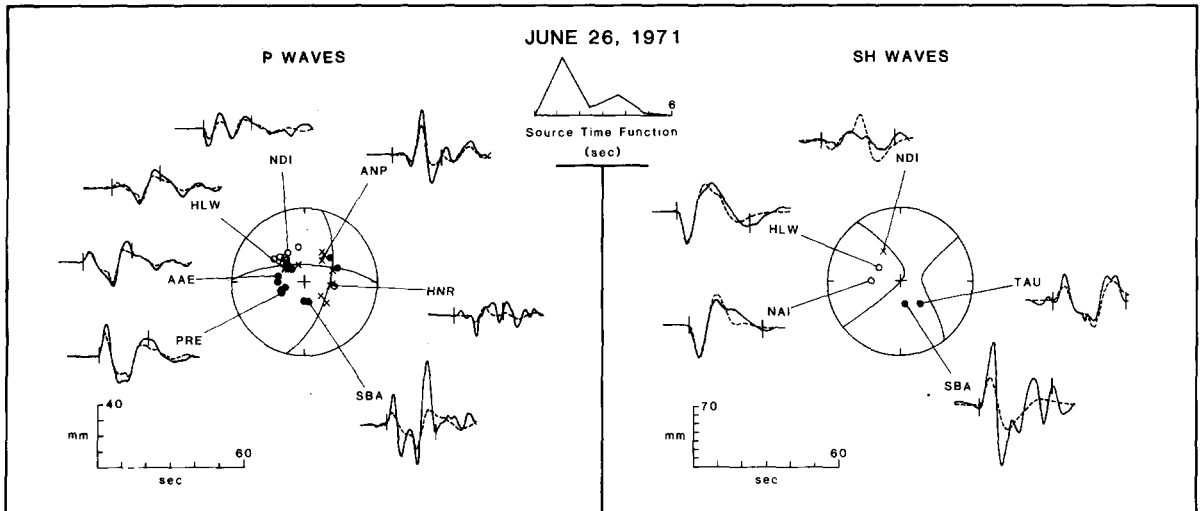


Fig. 6. Comparison of observed P and SH waves from the June 26, 1971 earthquake with synthetic waveforms generated for the best-fitting point source mechanism found in the body-waveform inversion. See Fig. 2 for further explanation.

terpretation, however, because the dominant trend in the bathymetry, at least to the south where it is not obscured by sediments, is NE-SW.

The SH waveforms from this earthquake can be matched well by synthetic waveforms calculated with a mechanism similar to that of Fitch, at a centroid depth of about 30 km. Such a solution provides a poor fit, however, to the observed P waveforms, whose complexity indicates that this earthquake consisted of several subevents. Our preferred solution (Fig. 5) consists of two point sources, at centroid depths of 27 and 39 km. Forward modeling indicated that the two subevents have nearly identical epicentroids (geographical location of the centroid); their horizontal separation was set to zero for the inversion. The two subevents occurred nearly simultaneously: the deeper subevent is delayed by only 0.6 s. Noting that the best-fitting single point-source solution is intermediate in depth between the two subevents in our preferred model, we infer that rupture initiated at a depth of between 30 and 35 km and propagated both upward and downward. The shallow part of the rupture has a nearly pure strike-slip mechanism (19/89/358) and a seismic moment of  $4.1 \times 10^{25}$  dyn-cm. The deeper subevent released about half as much seismic mo-

ment ( $2.1 \times 10^{25}$  dyn-cm) and has a small component of thrust faulting in its mechanism (32/73/21). The total seismic moment is  $6.1 \times 10^{25}$  dyn-cm. Richardson and Solomon (1977) estimated the moment to be  $6.7 \times 10^{25}$  dyn-cm from the spectral amplitudes of long-period SH waves. Stein and Okal (1978) reported a moment of only  $2.9 \times 10^{25}$  dyn-cm, but this value was estimated from the surface waves at one station.

### 3.5. June 26, 1971

The large earthquake on June 26, 1971 in the northeast Indian Ocean was studied by Sykes and Sbar (1974), who found a mechanism combining thrust faulting with a significant component of left-lateral strike-slip motion on a plane striking NNE. By matching observed P waveforms with synthetic waveforms generated using this mechanism, Wiens and Stein (1983) estimated a focal depth of 30 km, very close to the centroid depth of 29 km estimated in the inversion. The mechanism (14/67/19, Fig. 6) is very similar to the result of the first motion study. The seismic moment is  $5.4 \times 10^{25}$  dyn-cm. The horizontal component instruments at SBA were found to have reversed polarity, and the SH waveform was corrected prior to the inversion.

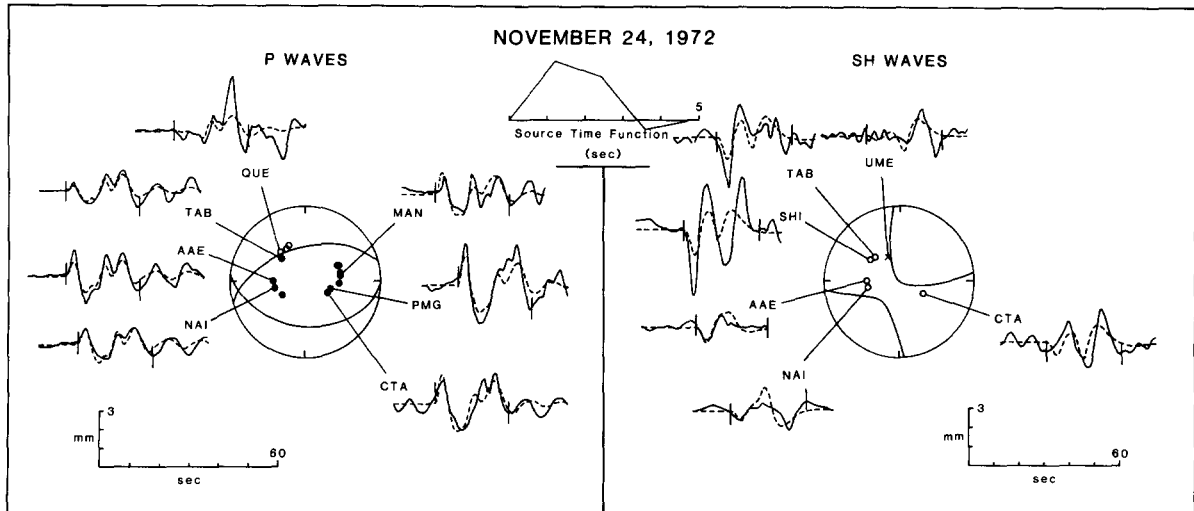


Fig. 7. Comparison of observed P and SH waves from the November 24, 1972 earthquake with synthetic waveforms generated for the best-fitting point source mechanism found in the body-waveform inversion. See Fig. 2 for further explanation.

### 3.6. November 24, 1972

The November 24, 1972 earthquake occurred beneath the eastern flank of the N–S trending  $85^{\circ}\text{E}$  Ridge (Liu et al., 1982) in the Bay of Bengal. For the inversion, the thick sedimentary layer in the epicentral region (Curry et al., 1982) was approximated by a 5 km thick layer with  $\alpha = 2.94 \text{ km s}^{-1}$ ,  $\beta = 1.60 \text{ km s}^{-1}$ , and  $\rho = 2.30 \text{ g cm}^{-3}$ . A study of the gravity anomaly over the  $85^{\circ}\text{E}$  Ridge indicates that it is probably a volcanic feature, formed on relatively young lithosphere (5–15 Ma) and buried when the lithosphere was 40–80 Ma old (Liu et al., 1982). The focal mechanism (254/52/76, Fig. 7) is characterized by thrust faulting with a P axis trending nearly N–S. The seismic moment is  $3.0 \times 10^{24} \text{ dyn-cm}$ . A centroid depth of 27 km below the sediment–water interface provides a good match to the observed P waveforms.

### 3.7. April 7, 1973

The large April 7, 1973 earthquake occurred on the northern end of the Ninetyeast Ridge, near its intersection with the western end of the Sunda Arc (Fig. 1). The station coverage and signal-to-noise ratio of the waveforms used in the inversion are

both excellent. The vertical and N–S horizontal component instruments at MAT were found to have reversed polarity; the observed P and SH waveforms were corrected accordingly. This earthquake is characterized by left-lateral strike-slip faulting on a plane which parallels the extinct NNE-trending spreading ridge segments thought to compose the northern part of the Ninetyeast Ridge (Curry et al., 1982), but the details of the waveforms cannot be matched satisfactorily with a single point source model. The synthetic waveforms shown in Fig. 8 were generated with a model consisting of two point sources. We inverted for the usual source parameters of each subevent plus the relative location and time delay of the second with respect to the first. The focal mechanisms of the two subevents are very similar, except that their strikes differ by  $14^{\circ}$  (34/84/356 and 20/87/9). The second subevent ( $M_0 = 8.3 \times 10^{25} \text{ dyn-cm}$ ) is about three times larger than the first ( $M_0 = 2.5 \times 10^{25} \text{ dyn-cm}$ ). In our preferred solution, the first subevent has a centroid depth of 13 km and the second, larger, event is at a depth of 6 km. Considering the strong tradeoff between source time function and centroid depth for strike-slip mechanisms and the masking effect of the second subevent, it is probable that an equally good fit to the observed waveforms could be

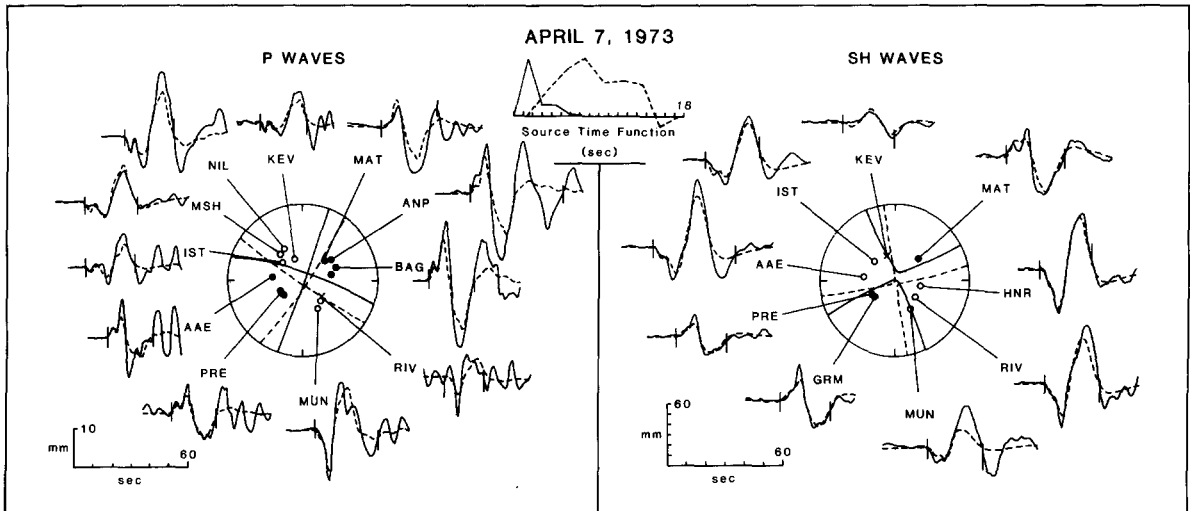


Fig. 8. Comparison of observed P and SH waves from the April 7, 1973 earthquake with synthetic waveforms generated with a model consisting of two point sources, the parameters of which were found in the body-waveform inversion. The dashed lines in the source time function and focal mechanisms represent the second subevent. The delay between the centroidal times of the subevents is shown; the apparent delay at any station depends on the angle between the line joining the subevents and the raypath. See Fig. 2 and the text for further explanation.

achieved with a model in which the first subevent is as shallow as the second. The epicentroid of the second subevent is about 14 km from the first at an azimuth of  $136^\circ$ , and delayed by 1.4 s. If the nodal planes striking NNE correspond to the fault planes, as one might expect from the tectonics of the source region, then the two subevents occurred on distinct, subparallel faults. We prefer this interpretation over the one in which the subevents both occurred on a single fault striking WNW.

### 3.8. August 30, 1973

The August 30, 1973 earthquake was located in the Bay of Bengal, directly east of Sri Lanka. Bergman and Solomon (1980) performed a first motion study of this event, finding a predominantly thrust-faulting mechanism with the P axis oriented NW-SE. As is usually the case for dip-slip mechanisms, the strikes of the nodal planes are poorly constrained by first motion data and they depend critically on the correct interpretation of emergent waveforms. In the source velocity structure for the inversion, we approximated the sediments of the Bengal Deep-Sea Fan by a 4.0 km thick layer with  $\alpha = 3.3 \text{ km s}^{-1}$ ,  $\beta = 1.9 \text{ km s}^{-1}$ ,

and  $\rho = 2.3 \text{ g cm}^{-3}$  (Curry et al., 1982). The focal mechanism found in the inversion (290/52/118, Fig. 9) has dip and slip angles very similar to the mechanism reported by Bergman and Solomon (1980), but the strike is rotated clockwise about  $40^\circ$  relative to the first motion solution. Weissel et al. (1980) showed only the direction of maximum principal stress for this event, but it appears they obtained a mechanism very similar to that of Bergman and Solomon (1980). Because of the small number of SH waveforms used in the inversion, the uncertainties in the orientation of the double couple are larger than usual, but the nearly N-S trend of the P axis is well constrained. The seismic moment is  $3.7 \times 10^{24} \text{ dyn-cm}$ .

It was difficult to find a centroid depth which satisfies simultaneously the P and SH waveforms. An inversion using only the P waveforms yields a centroid depth of about 24 km, very close to the depth of 23 km reported by Wiens and Stein (1983), but the separation of the direct S and sS phases at MAT and BUL requires a somewhat greater depth. A centroid depth of 27 km gives a good fit to these two SH waveforms and also provides a better fit to some of the P waveforms (e.g., JER and MSH) than the shallower solution,

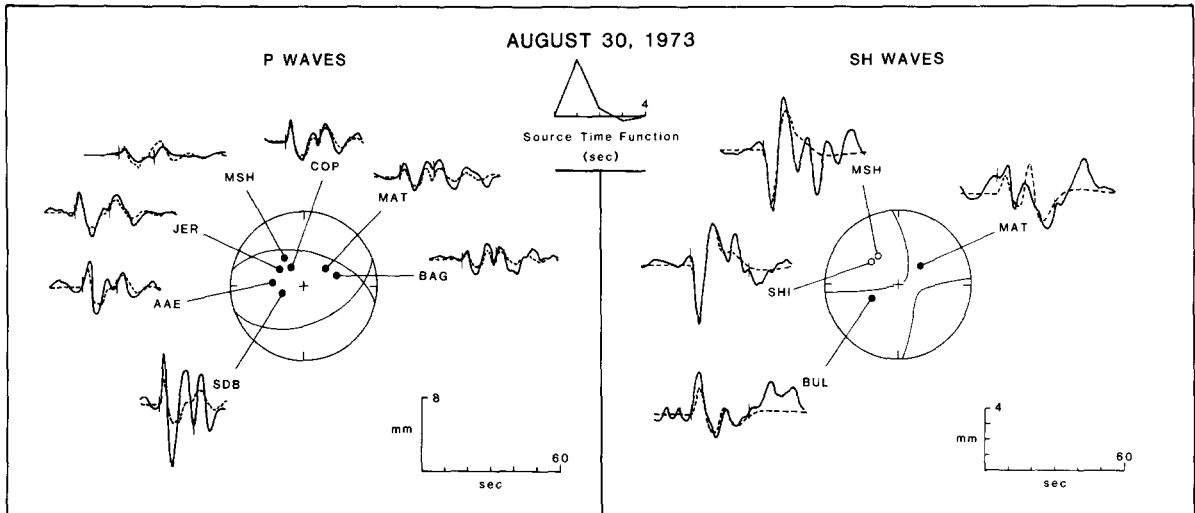


Fig. 9. Comparison of observed P and SH waves from the August 30, 1973 earthquake with synthetic waveforms generated for the best-fitting point source mechanism found in the body-waveform inversion. See Fig. 2 for further explanation.

and this is our preferred solution. The difficulty in converging to a single depth that matches both P and SH waveforms may reflect errors in the assumed velocity structure for the source.

### 3.9. June 25, 1974

The epicenter of the June 25, 1974 earthquake is in lithosphere created while the spreading direction in the central Indian Ocean was changing from approximately N-S to NE-SW, a setting similar to that of the September 14, 1968 event discussed above (Fig. 1). The source mechanism was first studied by Stein and Okal (1978), using first motion polarities to constrain one nodal plane to strike at  $242^\circ$  and dip to the northwest at about  $74^\circ$ . Stein and Okal (1978) used the Love wave radiation pattern to estimate a slip angle of about  $97^\circ$  and a seismic moment of  $2.5 \times 10^{25}$  dyn-cm. Such a mechanism represents near-vertical dip-slip faulting on a plane similar in strike to the fracture zone to the southeast, in which case differential subsidence on the fracture zone would be a likely source for the stress relieved in this earthquake.

The mechanism proposed by Stein and Okal (1978), however, produces a very poor fit to the observed P and SH waves. In fact, we found no single point source mechanism which produces a

satisfactory fit to both the P and SH waveforms. The point source mechanism found in an inversion using only SH waves (9/67/8,  $M_0 = 1.4 \times 10^{26}$  dyn-cm, with a source time function about 16 s in duration and a centroid depth of 20 km, Fig. 10) represents nearly pure left-lateral strike-slip faulting on a plane striking slightly east of north, parallel to the fracture zone north of the epicentral region. The source time function has three distinct pulses, suggesting considerable complexity in the rupture process. This mechanism produces synthetic P waveforms which are much smaller than the observed waveforms, however (Fig. 10). Conversely, the major features of most of the P waveforms (but not the SH waveforms) can be reproduced by a thrust-faulting mechanism similar to the mechanism proposed by Stein and Okal (1978), but with a shallower dip angle.

The observed P and SH waveforms from this earthquake can be matched simultaneously only with a model consisting of at least two point sources, one characterized by strike-slip motion and the other dominated by thrust faulting. The largest fraction of the seismic moment release for this event occurred in two such subevents, the strike-slip component having a duration of about 6 s and the thrust faulting component having a duration of about 3 s. The observed waveforms are

fit much more convincingly, however, by models in which the rupture continues at a lower level for another 10–15 s. We performed inversions with a variety of parameterizations, ranging from models consisting of two point sources with long source time functions to models with as many as four point sources, to try to resolve the rupture process of the later part of the earthquake. None of these models was found to be conspicuously better than any other, as long as there is provision for a low level of seismic moment release up to about 20 s after the initiation of rupture.

Our preferred mechanism consists of three sub-events, the first of which (with the largest component of strike-slip motion) has a long time function containing three fairly distinct pulses. This was a consistent feature of successful models, which we take to be further evidence for source multiplicity. Satisfactory two-source models require a second (thrust faulting) subevent with a long time function, generally characterized by an initial pulse of several seconds duration followed by one or more distinct pulses. However, the later part of the source time function of this second subevent is quite unstable. Although the three-source model presented here is not statistically superior to the best two-source model (if the second subevent is

given a sufficiently long time function), we feel it better represents the faulting history of this earthquake, which apparently occurred as a number of small, nearly simultaneous subevents with rather variable focal mechanisms. The details of such a source are extremely difficult to resolve with long-period teleseismic waveform data. We inverted for the usual source parameters for each of the three subevents plus the relative location of each subevent's centroid with respect to the initial rupture, using the observed short-period arrival time as a reference point for each P waveform. For the second and third subevents, we also inverted for the centroid time delay relative to the initial rupture.

The first subevent is similar to the strike-slip mechanism which produces a good fit to the SH waves (10/50/25,  $M_0 = 1.1 \times 10^{26}$  dyn-cm,  $h = 23$  km). The total length of the source time function for this subevent is about 20 s, but the rate of seismic moment release is small following the two distinct pulses in the first 8 s. The shape of the source time function of the first subevent was surprisingly consistent through all the trial inversions. The P waveforms are dominated by the second, predominantly thrust-faulting subevent (47/53/73,  $M_0 = 2.6 \times 10^{25}$  dyn-cm,  $h = 18$  km),

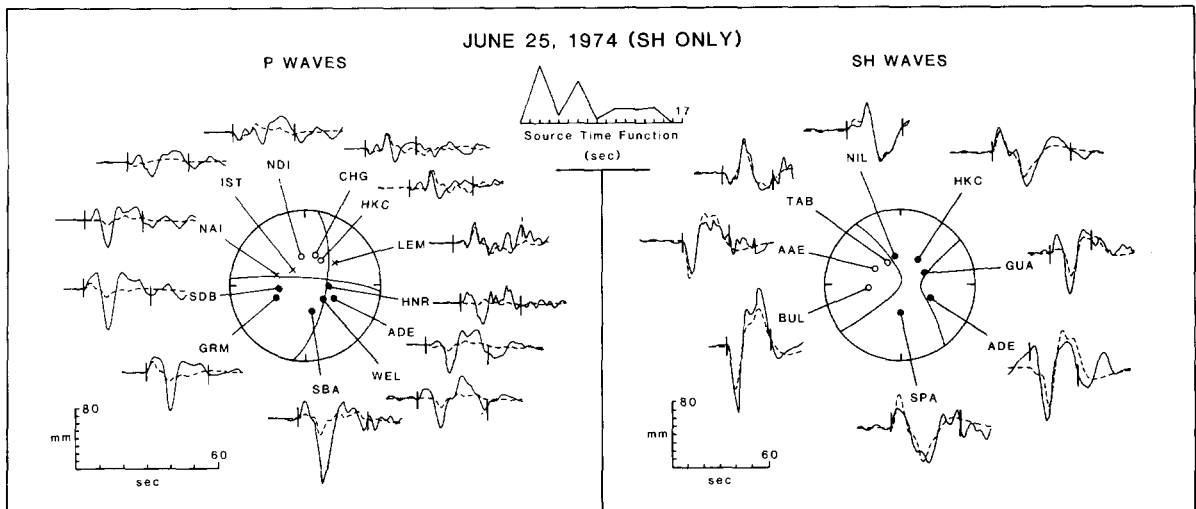


Fig. 10. Comparison of observed P and SH waves from the June 25, 1974 earthquake with synthetic waveforms generated for the best-fitting point source mechanism found when SH waves only are used in the body-waveform inversion. See Fig. 2 for further explanation.

which is delayed by 2.6 s. The epicentroid of this subevent is about 11 km southwest (azimuth  $234^\circ$ ) of the first subevent. The third subevent has a mechanism intermediate between those of the first two subevents (36/48/41), a centroid depth of 13 km, and a moment of  $1.1 \times 10^{25}$  dyn-cm. Its epicentroid is 9 km north (azimuth  $347^\circ$ ) of the first subevent and delayed by 9 s. Trial inversions indicated that the second subevent lasted about 3 s; to reduce the number of free parameters, the source time function was parameterized as a single triangle 3 s in duration. The source time function of the third subevent was also parameterized as a 3 s triangle, but within rather broad limits the source time function of this subevent is unresolvable. The estimated source parameters of the second and third subevents, particularly the third, have larger uncertainties than usual because the signals from the later subevents are obscured by the waveforms of the first. The total moment for this event is  $1.5 \times 10^{26}$  dyn-cm, six times larger than that estimated by Stein and Okal (1978). The observed P and SH waveforms and the synthetic waveforms generated with this multiple source model are shown in Fig. 11.

Our tectonic interpretation of this event is based on the observation that it occurred in oceanic lithosphere which is likely to have an unusually complex structure. Because of the major change in spreading direction which occurred during the creation of the lithosphere in the epicentral region, we expect an abnormally large number of pre-existing faults in the crust and upper mantle. Faults with strikes subparallel to the two dominant fracture zone trends in the region, approximately  $N10^\circ E$  and  $N45^\circ E$  (Fig. 1), should be especially common. The source parameters inferred for the June 25, 1974 earthquake are consistent with the deformation of such a structurally complex region in response to a regional stress field characterized by N-S compression and left-lateral shear on planes striking N-S. In this earthquake, rupture occurred almost simultaneously on a number of small faults. Instead of a mixture of thrust faulting events and strike-slip events, most of the subevents had combination mechanisms with the amount of thrust faulting in each subevent controlled by the orientation of the fault plane; thrusting increases as the fault strike increases clockwise from north.

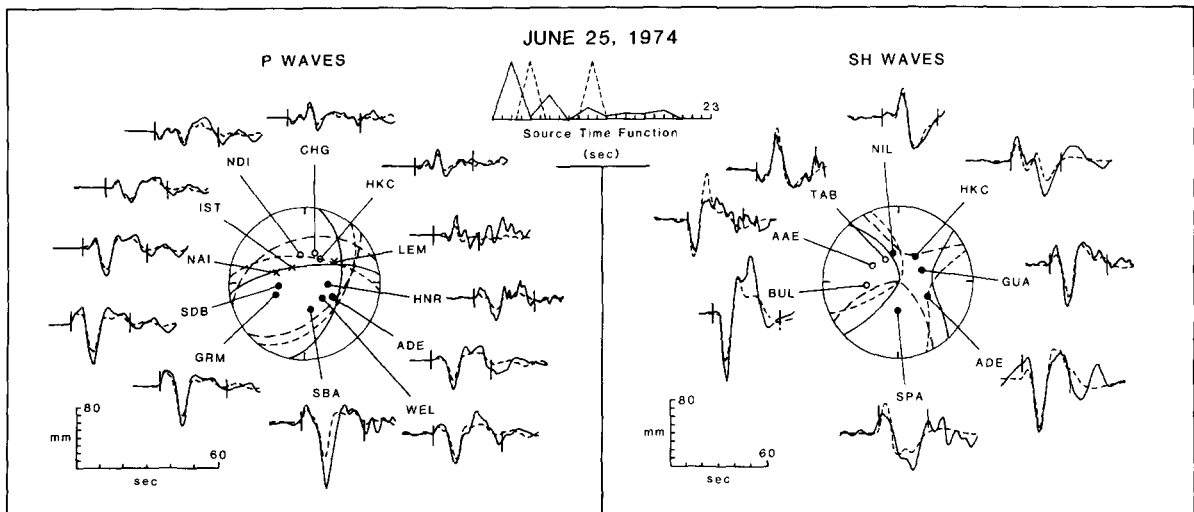


Fig. 11. Comparison of observed P and SH waves from the June 25, 1974 earthquake with synthetic waveforms generated for a source model consisting of three point sources, the parameters of which were found in the body-waveform inversion. The long and short dashed nodal lines in the focal mechanisms represent the second and third subevents, respectively. The source time function of the first subevent is shown by a solid line; a triangular time function 3 s in duration was used for the second and third subevents. The delays between the centroidal times of the three subevents are shown; the apparent delays at any station depend on the angles between the lines joining the subevents and the raypath. See text and Fig. 2 for further explanation.

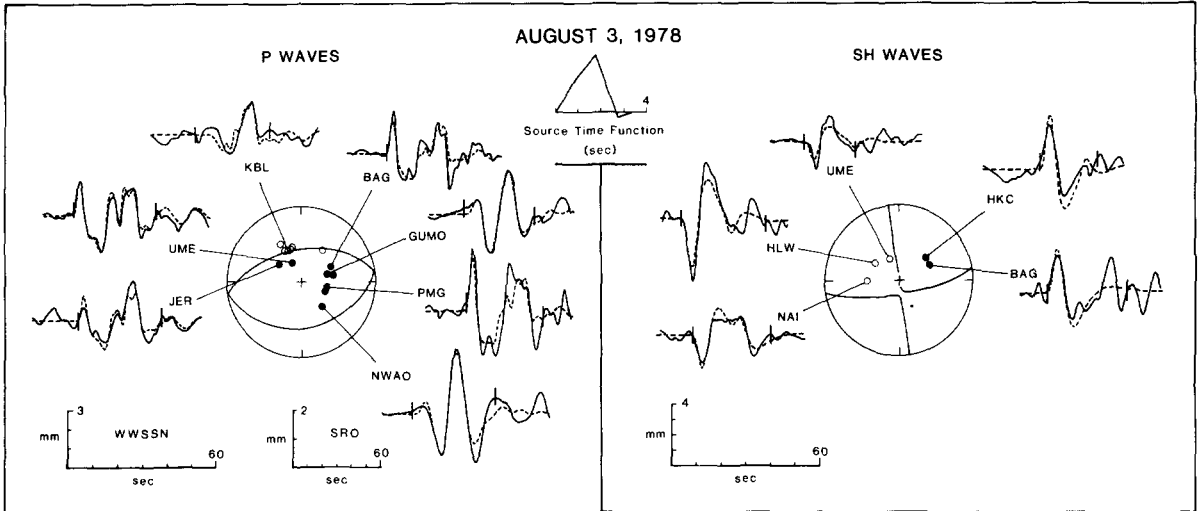


Fig. 12. Comparison of observed P and SH waves from the August 3, 1978 earthquake with synthetic waveforms generated for the best-fitting point source mechanism found in the body-waveform inversion. Waveforms recorded at GDSN stations (NWAO and GUMO) are plotted with a separate time-amplitude scale. See Fig. 2 for further explanation.

3.10. August 3, 1978

The August 3, 1978 earthquake was located west of the Ninetyeast Ridge in an area which has been very active seismically over the last two decades (Fig. 1) and in which Weissel et al. (1980) observed other evidence of recent large-scale deformation. Weissel et al. (1980) indicated that this

event is characterized by thrust faulting with a P axis oriented slightly west of north, but they do not report the focal mechanism. Using forward modeling of P waveforms, Bergman and Solomon (1982) found a similar mechanism and estimated the depth to be about 40 km below the seafloor, making it one of the deepest known oceanic intraplate earthquakes. From a similar analysis,

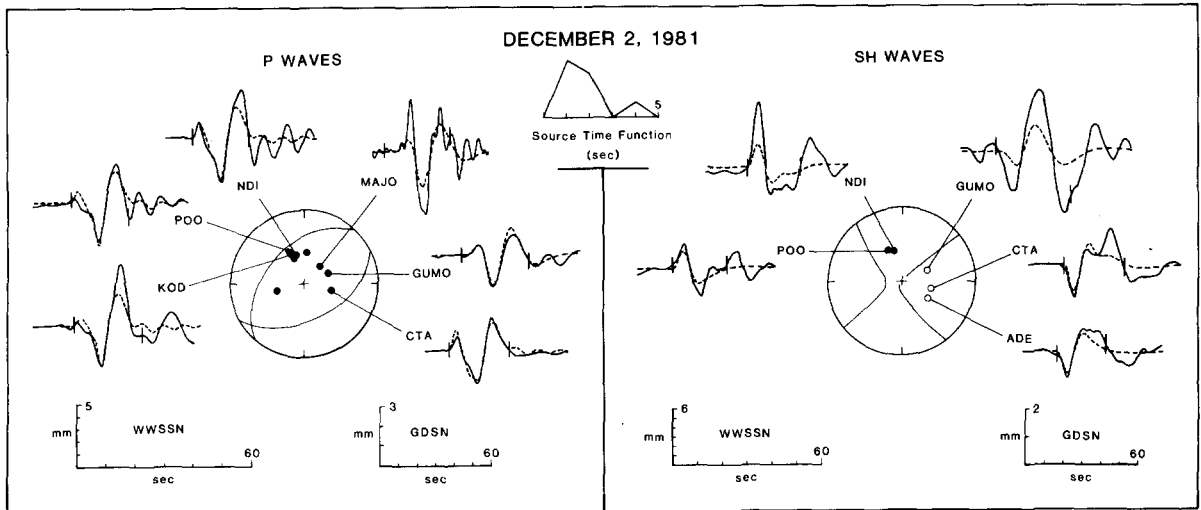


Fig. 13. Comparison of observed P and SH waves from the December 2, 1981 earthquake with synthetic waveforms generated for the best-fitting point source mechanism found in the body-waveform inversion. Waveforms recorded at GDSN stations (MAJO and GUMO) are plotted with a separate time-amplitude scale. See Fig. 2 for further explanation.

Wiens and Stein (1983) also obtained a thrust-faulting mechanism (265/57/90) and a depth of 40 km. Station coverage is reasonably good for this event and the inversion converged very quickly to a pure thrust-faulting mechanism (261/53/90, Fig. 12), at a depth of 39 km. The seismic moment is  $5.9 \times 10^{24}$  dyn-cm.

### 3.11. December 2, 1981

The epicenter of the December 2, 1981 earthquake is on the eastern flank of the Ninetyeast Ridge, at the latitude of the Osborn Knoll (Fig. 1). Dziewonski and Woodhouse (1983) obtained the following source parameters from an inversion of GDSN data:  $M_0 = 5.0 \times 10^{24}$  dyn-cm, focal mechanism = 192/49/34, with the depth fixed at 10 km. Using WWSSN data in addition to several GDSN stations, we determined a centroid depth of 23 km and a mechanism characterized by a larger component of thrust faulting (222/44/78, Fig. 13). Station coverage is rather poor, and the uncertainties in the source parameters are therefore larger than usual. The seismic moment determined in the body-waveform inversion ( $5.8 \times 10^{24}$  dyn-cm) is in close agreement with the previous estimate.

## 4. Internal deformation of the Indian plate

The portion of the Indian plate under consideration here is quite large, has a complex and incompletely understood tectonic history, and is currently undergoing internal deformation, probably in several distinct modes. The seismological data set available to investigate this deformation consists of the 11 source mechanisms discussed above and focal mechanisms of two older earthquakes (1939 and 1955) obtained by Stein and Okal (1978). Interpretations of the pattern of seismicity in this region are known to be subject to bias from too brief a span of observations (e.g., Sykes, 1970). Similarly, the focal mechanisms of a small subset of these earthquakes may be unrepresentative of the long-term average seismogenic deformation of the lithosphere in the northern Indian Ocean. In fact, we as yet have little knowledge of what the

appropriate time scale for such a long-term average model might be.

During the last several decades, the intraplate seismicity of the northern Indian Ocean has been dominated by thrust faulting on E–W striking faults and left-lateral strike-slip motion on faults striking N–S. Stein and Okal (1978) reported a normal faulting mechanism for the large March 22, 1955 earthquake, on the eastern side of the Ninetyeast Ridge in lithosphere about 55 Ma old, but the analysis was based on a very small set of surface waves and first motion polarities of questionable reliability. A good example of the potential for error in a source study of this type is the June 25, 1974 earthquake discussed above. The data available for the 1974 event were far superior to those used in the source study of the 1955 earthquake. With the exception of earthquakes representing the release of bending stresses seaward of trenches, no earthquake in oceanic lithosphere older than about 35 Ma has been found to have a normal-faulting mechanism (Wiens and Stein, 1983; Bergman, 1984). Furthermore, there is no satisfactory explanation for the occurrence of normal faulting east of the Ninetyeast Ridge, while the observed faulting styles of the other earthquakes in the region can all be accommodated within the framework of a general model of the deformation of the Indian plate first suggested by Stein and Okal (1978). The additional earthquake source mechanisms presented here are consistent with the basic elements of that model. Unless and until an unambiguous example of normal faulting is found in this area, we presume that the mechanism of the 1955 earthquake is essentially unconstrained.

The basic premise of the model suggested by Stein and Okal (1978) for the deformation of the Indian plate is that the northern part of the Ninetyeast Ridge is the site of at least partial decoupling between the Indian and Australian halves of the plate, prompted by the great change in plate boundary type which occurs at this longitude. East of the Ninetyeast Ridge, the plate encounters little resistance as it is subducted at the Sunda Arc. To the west, however, the northward movement of the Indian half of the plate is impeded by the continental collision with Asia. The expected result of

this system of forces on the northern plate boundary is left-lateral shear stress (on a N-S plane) in the vicinity of the Ninetyeast Ridge, as represented by the focal mechanism of the May 25, 1964 earthquake and to a lesser extent, the mechanism proposed by Stein and Okal (1978) for the March 21, 1939 earthquake. The mechanism of the April 7, 1973 earthquake indicates that this left-lateral strike-slip motion on the Ninetyeast Ridge presently extends to the northern termination of the ridge at the western end of the Sunda Arc (Fig. 1).

The southern extent of strike-slip faulting on the Ninetyeast Ridge is less clear. The December 2, 1981 earthquake at about 16°S is the only large earthquake on the Ninetyeast Ridge south of the May 1964 event, and it is characterized by thrust faulting with a P axis oriented NW-SE (Fig. 1). At 26°S and a short distance west of the Ninetyeast Ridge, however, the major component of the complex June 25, 1974 earthquake is left-lateral strike-slip faulting on a N-S plane, presumably the fracture zone inferred at this site by Sclater and Fisher (1974). If this event is responding to the same stress system which produces strike-slip faulting on the northern part of the Ninetyeast Ridge, we must expect that the southern half of the Ninetyeast ridge occasionally experiences strike-slip faulting as well.

To the east of the Ninetyeast Ridge the level of seismicity declines. The two earthquakes in this region with known focal mechanisms (June 26, 1971 and October 31, 1965) are both characterized by left-lateral strike-slip motion on nodal planes oriented within about 15° of N-S (Fig. 1). The trend of the bathymetry in the epicentral region of the 1971 event parallels the nodal plane striking N13°E, and this nodal plane probably corresponds to the fault plane, but there is little basis for selecting one of the nodal planes of the 1965 earthquake as the fault plane.

The source mechanisms of earthquakes to the west of the Ninetyeast Ridge are consistent with N-S shortening in a compressive stress field. Three of the four earthquakes north of about 5°S are characterized by thrust faulting with the P axis oriented close to N-S (Fig. 1). Dziewonski et al. (1984) also reported a predominantly thrust-fault-

ing mechanism (254/77/71) with a P axis striking N-S for a small earthquake located at 2.76°N, 87.29°E on August 21, 1983. The epicenter is further east than the other known thrust-faulting events, near the western flank of the Ninetyeast Ridge.

The shallower subevent ( $h = 27$  km) of the October 1970 earthquake has a pure left-lateral strike-slip mechanism on a vertically-dipping plane striking N19°E, close to the trend of the fracture zone which passes through the epicentral area (Fig. 1). For this reason and because of the obvious similarity to the style of deformation on the Ninetyeast Ridge, we take this nodal plane to correspond to the fault plane. The P axis for this subevent is oriented N26°W. A better estimate of the true direction of maximum compressive stress, however, can be made when the fault plane is known. According to the criterion of Raleigh et al. (1972), the best estimate of the direction of greatest compression may be found by rotating the P axis about 15° toward the slip vector. For the shallow subevent, we estimate an orientation of N11°W for the maximum compressive stress, consistent with the directions inferred from the thrust-faulting mechanisms of the other events west of the Ninetyeast Ridge. A similar analysis of the mechanism of the deeper subevent ( $h = 39$  km), which has a small component of thrust motion (consistent with north-south compression), leads to an estimate of N2°W for the direction of maximum compressive stress.

There is very little seismicity to the west of the Ninetyeast Ridge between latitudes 4°S and 24°S, but both earthquakes (September 1968 and June 1974) in the southwestern part of the study area have at least a component of thrust faulting (Fig. 1). The September 1968 earthquake is quite small and one of the few oceanic intraplate events known to have occurred in the crust (Wiens and Stein, 1983; Bergman, 1984). We suggest below that this event may have released stresses associated with the elevated topography of the Southeast Indian Ridge. With the present data, the degree to which these earthquakes represent a southward continuation of the distinctive pattern of seismicity and source mechanisms observed in the Bay of Bengal is uncertain.

An obvious cause of N-S compression and shortening of the lithosphere to the west of the Ninetyeast Ridge is the continental collision between India and Asia. Weissel et al. (1980) and Geller et al. (1983) suggested a connection between the Late Miocene onset of the Himalayan orogeny and the principal stress directions of intraplate earthquakes, unusually high heat flow, and deformational structures in the crust and sediments of the northern Indian Ocean. The mechanism presented here for the November 24, 1972 earthquake increases the latitudinal extent of the zone of compressional deformation to over 1000 km (from just south of the equator to at least 11°N).

The source parameters derived in this study provide new constraints on the nature of this intraplate deformation zone. The centroid depths of the three thrust-faulting events west of the Ninetyeast Ridge are 27 km (November 1972 and August 1973) and 39 km (August 1978) below the seafloor. The two subevents of the October 1970 strike-slip event have centroid depths of 27 and 39 km. The focal mechanisms and centroid depths of these earthquakes, in combination with the shallow deformational structures observed by Weissel et al. (1980), suggest that the mechanism of deformation involves compressional failure at all depths within the portion of the lithosphere capable of sustaining significant differential stress. Alternative explanations for the observed undulation in the oceanic crust and sediments involve buckling or folding of a substantial portion of the elastic lithosphere (Weissel et al., 1980; McAadoo and Sandwell, 1984). Simple models of lithospheric buckling require a horizontal compressive deviatoric stress well in excess of the strength of the lithosphere (Weissel et al., 1980). Lithospheric folding models with substantially lower magnitudes for the buckling stress (McAadoo and Sandwell, 1984) have difficulty explaining the absence of earthquakes indicative of normal faulting in regions where bending stresses are predicted to be large and extensional; for example, a 14 km thick plate folded at a predominant wavelength of 200 km with a fold amplitude of 1 km (Weissel et al., 1980) experiences a maximum extensional bending stress in excess of 7 kbar.

Noting several recent examples where major thrust-faulting earthquakes were concealed beneath active fold systems, King and Stein (1984) suggested that such folding may be a consequence of diminished fault slip at shallow depths. The absence of shallow thrust-faulting earthquakes in the Bay of Bengal is consistent with such a hypothesis, but the mechanism through which thrust faulting at depth could produce the spatial regularity observed in the crustal deformation (Weissel et al., 1980) is unknown.

## 5. State of stress in the Indian plate

The relatively large number of intraplate earthquakes with known focal mechanisms in the northern Indian Ocean provides an excellent opportunity to test for large-scale features in the intraplate stress field. It also allows us to consider the accuracy with which any single focal mechanism reflects the regional stress pattern inferred from a number of earthquake mechanisms.

Supplementing the few oceanic intraplate earthquake mechanisms then available with data from India and Australia, Fitch (1972) and Fitch et al. (1973) proposed that the various indicators of stress delineated a single long-wavelength feature of the intraplate stress field: the orientation of the greatest horizontal compressive stress is oriented roughly N-S in India, swings to NW-SE in the northern Indian Ocean and is nearly E-W in Australia. Bergman and Solomon (1980) and Weissel et al. (1980) presented further support for this hypothesis.

With the earthquake source studies reported here, we now have a larger (and more accurate) set of focal mechanisms with which to investigate the regional stress field in the northern Indian Ocean. The directions of maximum horizontal compressive stress inferred from the focal mechanisms of these events are plotted in Fig. 14. For thrust-faulting events, the strike of the horizontal projection of the P axis has been plotted. In the case of the seven strike-slip events for which fault planes can be specified with some confidence (May 25, 1964, June 26, 1971, both subevents of the April 7, 1973 event, the first subevent of the June

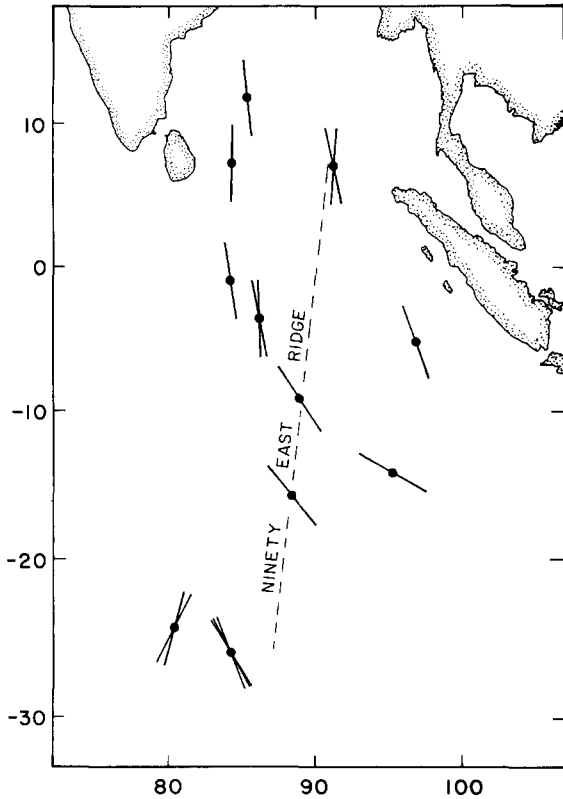


Fig. 14. Map of the orientation of maximum horizontal compressive stress in the northern Indian Ocean, inferred from the focal mechanisms listed in Table I (see text).

25, 1974 earthquake, and both subevents of the October 10, 1970 earthquake), we have estimated the orientation of the maximum horizontal compressive stress according to the criterion of Raleigh et al. (1972), as discussed above. The horizontal projection of the P axis of the October 31, 1965 earthquake has been plotted, since we found no basis for selecting one of the nodal planes as the fault plane for that event.

The principal stress orientations shown in Fig. 14 confirm and refine the results of previous studies. The data available to Bergman and Solomon (1980), for example, supported a general NW-SE trend to the stress field, but no curvature of stress trajectories was observable. In the present study we have modified several of the previously reported mechanisms, obtained several new mechanisms, and used an improved technique to infer the orientation of principal stresses from focal

mechanisms. Figure 14 clearly indicates a curvature in the regional stress field, with the direction of maximum horizontal stress changing from about  $N10^{\circ}W$  in the Bay of Bengal to approximately  $N45^{\circ}W$  to the east of the Ninetyeast Ridge. The Ninetyeast Ridge appears to have little or no influence on the inferred direction of the greatest compressive stress, although there is a gap in the data in the immediate vicinity of the northern part of the ridge. This image of the intraplate stress field is fully consistent with the original proposal of Fitch (1972) and also with numerical models of the intraplate stress field in the Indian plate based on assumed plate boundary forces (Richardson et al., 1979).

The direction of maximum horizontal stress (NNE) inferred for the small September 1968 earthquake, in the southern part of the study area, varies somewhat from the regional pattern observed to the north. The P axis of this event is nearly perpendicular to the nearby Southeast Indian Ridge, suggesting that the earthquake may have released compressive stress associated with the elevated ridge topography ("ridge push"). The 1968 earthquake is one of the few oceanic intraplate events known to have occurred in the crust, where stresses from elevated ridge topography should be largest (Dahlen, 1981). For the 1968 event, Dahlen's model predicts a maximum horizontal deviatoric compressive stress of about 200 bars at the seafloor. The state of stress inferred from this shallow event may not be representative of the stress at deeper levels in the lithosphere at the same site, because the relatively weak crust is incapable of transmitting large deviatoric stresses over great distances. The much larger earthquake on June 25, 1974, a short distance to the east of this event, occurred in the upper mantle and the direction of maximum horizontal compressive stress inferred from its mechanism is in better agreement with the pattern observed to the north (Fig. 14).

In the northern Indian Ocean, the focal mechanisms of intraplate earthquakes appear to be reliable indicators of the orientation of principal intraplate stresses, even though the region is experiencing significant internal deformation in at least two distinct modes. This result does not justify,

however, the uncritical use of intraplate earthquake focal mechanisms to “map” the long-wavelength tectonic stress field in other oceanic regions. Oceanic intraplate events in other regions may be influenced primarily by locally-produced stresses which have no relation to the plate-wide stress field. Further, the consistency of stresses inferred from focal mechanisms in the northern Indian Ocean may be the result of unusually large and homogeneous deviatoric stresses throughout a large volume of lithosphere, a product of the peculiar boundary conditions on the Indian plate. Because the typical level of long-wavelength stress differences in other oceanic regions is likely to be lower, intraplate earthquakes elsewhere need not be comparably reliable indicators of plate-wide stresses.

## 6. Conclusions

Detailed source mechanisms of 11 intraplate earthquakes provide constraints on the state of stress and style of deformation of the oceanic lithosphere in the northern Indian Ocean, the most seismically active oceanic intraplate region. Double-couple point source parameters of the earthquakes were determined with a formal inversion technique (Nabelek, 1984) based on a least-squares fit of synthetic waveforms to observed teleseismic long-period P and SH waveforms. The use of short-period P waveforms significantly improved the resolution of the centroid depth and rupture history for the smallest event studied. Multiple point-source models were required to match satisfactorily the observed waveforms for four of the earthquakes.

All 11 earthquakes are characterized by either thrust or strike-slip faulting (or a combination of the two). The seismogenic deformation of the oceanic lithosphere in the northern Indian Ocean can be characterized by defining several intraplate tectonic provinces, similar to the “stress provinces” defined for the conterminous U.S. by Zoback and Zoback (1980). These tectonic provinces are distinguished on the basis of level of seismicity, inferred stress directions, and style of faulting. In the Bay of Bengal, from just south of the equator

to at least 11°N, intraplate earthquakes have thrust-faulting mechanisms on fault planes striking E–W. Earthquakes along the northern part of the Ninetyeast Ridge display left-lateral strike-slip faulting on planes striking N–S, parallel to the ridge. This style of faulting is observed from the very northern end of the Ninetyeast Ridge (7°N), where it intersects the Sunda Arc, to as far south as 10°S. Thrust faulting indicating NW–SE compression is observed on the Ninetyeast Ridge at 16°S. To the east of the Ninetyeast Ridge the level of seismicity drops and the earthquakes are characterized by mechanisms combining the thrust and strike-slip motion observed in the Bay of Bengal and along the northern part of the Ninetyeast Ridge, respectively. In the southern part of the study area, approaching the Southeast Indian Ridge, earthquake mechanisms are dominated by thrust and strike-slip faulting of the sort observed to the north, but there is a large intervening region which has been relatively aseismic during recent decades. The southern extent of the distinctive intraplate tectonic provinces of the northern Indian Ocean is, therefore, uncertain.

The overall pattern of seismogenic deformation in the northern Indian Ocean is consistent with the tectonic model proposed by Stein and Okal (1978), in which the northern part of the Ninetyeast Ridge is the site of partial decoupling between the Indian and Australian halves of the plate. In that model, the deformation is driven by the abrupt change in boundary conditions along the northern margin of the plate at the longitude of the Ninetyeast Ridge, with a continental collision zone to the west and an oceanic subduction zone to the east.

Thrust faulting earthquakes in the Bay of Bengal occur at depths between 25 and 40 km below the seafloor. No crustal-level earthquakes have been observed, although other lines of evidence indicate active compressional deformation, apparently by folding, of the sedimentary and upper crustal layers (Weissel et al., 1980). Such folding is unlikely to extend deep into the lithosphere, since the stress necessary to cause buckling of a significant portion of the lithosphere has been shown to be unrealistically large (Weissel et al., 1980). It appears therefore that compression and shortening of the lithosphere in this region may be accom-

modated by folding only at crustal levels, while thrust faulting dominates the deformation in the upper mantle. One explanation for these observations is that shallow folding may be caused by thrust-faulting at depth if the rupture fails to reach the surface (King and Stein, 1984).

Principal stress directions inferred from the focal mechanisms of these earthquakes display a consistent long-wavelength pattern, in which the direction of maximum horizontal compressive stress changes smoothly from slightly west of north in the Bay of Bengal to NW–SE in the northeastern Indian Ocean. Such a pattern is consistent with the stress field predicted by numerical models of the intraplate stress field in the Indian plate with simply-parameterized boundary forces (Richardson et al., 1979). The consistency with which the mechanisms of individual earthquakes reflect this pattern may be at least partly the result of unusually large plate-wide deviatoric stresses associated with the Himalayan orogeny. In regions where the long-wavelength part of the stress field is comparable in magnitude to locally-produced stresses, oceanic intraplate earthquakes may be less reliable indicators of the plate-wide tectonic stress field.

#### Note added in proof

Cloetingh and Wortel (1985) have recently published a finite-element model of stress in the Indian plate incorporating distributed ridge-push and boundary forces at subduction zones that depend on the age of subducted lithosphere. Their model is consistent both with the principal stress directions in Fig. 14 and with a higher level of deviatoric stress in the northern Indian Ocean than is typical of other oceanic intraplate settings.

#### Acknowledgments

We thank Jan Nattier-Barbaro for help with manuscript preparation and Jean Kahl for drafting. This research was supported by the National Aeronautics and Space Administration under grant NAG5-44 and contract NAS 5-27339 and by the

National Science Foundation under grant EAR-8115908.

#### References

- Aki, K. and Richards, P.G., 1980. *Quantitative Seismology: Theory and Methods*. Vol. 1. W.H. Freeman, San Francisco, 557 pp.
- Banghar, A.R. and Sykes, L.R., 1969. Focal mechanisms of earthquakes in the Indian Ocean and adjacent regions. *J. Geophys. Res.*, 74: 632–649.
- Bergman, E.A., 1984. *Intraplate earthquakes and the state of stress in oceanic lithosphere*. Ph.D. Thesis, Mass. Inst. of Technol., Cambridge, 448 pp.
- Bergman, E.A. and Solomon, S.C., 1980. Oceanic intraplate earthquakes: implications for local and regional intraplate stress. *J. Geophys. Res.*, 85: 5389–5410.
- Bergman, E.A. and Solomon, S.C., 1982. Recent studies in Indian Ocean intraplate seismicity. *EOS Trans. Am. Geophys. Union*, 63: 1092 (abstract).
- Bergman, E.A. and Solomon, S.C., 1984. Source mechanisms of earthquakes near mid-ocean ridges from body waveform inversion: implications for the early evolution of oceanic lithosphere. *J. Geophys. Res.*, 89: 11,415–11,441.
- Bergman, E.A., Nabelek, J.L. and Solomon, S.C., 1984. An extensive region of off-ridge normal-faulting earthquakes in the southern Indian Ocean. *J. Geophys. Res.*, 89: 2425–2443.
- Bowin, C., 1973. Origin of the Ninetyeast Ridge from studies near the equator. *J. Geophys. Res.*, 78: 6029–6043.
- Cloetingh, S. and Wortel, R., 1985. Regional stress field of the Indian plate. *Geophys. Res. Lett.*, 12: 77–80.
- Cormier, V.F., 1982. The effect of attenuation on seismic body waves. *Bull. Seismol. Soc. Am.*, 72: S162–S200.
- Curry, J.R., Emmel, F.J., Moore, D.G. and Raitt, R.W., 1982. Structure, tectonics, and geological history of the northeastern Indian Ocean. In: A.E.M. Nairn and F.G. Stehli (Editors), *The Ocean Basins and Margins: The Indian Ocean*. Plenum-Press, New York, 6: 399–450.
- Dahlen, F.A., 1981. Isostasy and the ambient state of stress in the oceanic lithosphere. *J. Geophys. Res.*, 86: 7801–7807.
- Das, S. and Aki, K., 1977. Fault planes with barriers: a versatile earthquake model. *J. Geophys. Res.*, 82: 5658–5670.
- Der, Z.A., McElfresh, T.W. and O'Donnell, A., 1982. An investigation of the regional variations and frequency dependence of anelastic attenuation in the mantle under the United States in the 0.5–4 Hz band. *Geophys. J. R. Astron. Soc.*, 69: 67–100.
- Detrick, R.S., Sclater, J.G. and Thiede, J., 1977. The subsidence of aseismic ridges. *Earth Planet. Sci. Lett.*, 34: 185–196.
- Dziewonski, A.M. and Woodhouse, J.H., 1983. An experiment in systematic study of global seismicity: centroid-moment tensor solutions for 201 moderate and large earthquakes of 1981. *J. Geophys. Res.*, 88: 3247–3272.
- Dziewonski, A.M., Franzen, J.E. and Woodhouse, J.H., 1984.

- Centroid-moment tensor solutions for July–September, 1983. *Phys. Earth Planet. Inter.*, 34: 1–8.
- Ebel, J. and Helmlinger, D.V., 1982. P wave complexity and fault asperities: the Borrego mountain earthquake of 1968. *Bull. Seismol. Soc. Am.*, 72: 413–438.
- Fisher, R.L., Jantsch, M.Z. and Comer, R.L., 1982. General Bathymetric Chart of the Oceans (GEBCO). Canadian Hydrographic Service, Ottawa, Sheet 5.09, 5th ed.
- Fitch, T.J., 1972. Plate convergence, transcurrent faults, and the internal deformation adjacent to Southeast Asia and the western Pacific. *J. Geophys. Res.*, 77: 4432–4460.
- Fitch, T.J., Worthington, M.H. and Everingham, I.B., 1973. Mechanisms of Australian earthquakes and contemporary stresses in the Indian Ocean plate. *Earth Planet. Sci. Lett.*, 18: 345–356.
- Francis, T.J.G. and Raitt, R.W., 1967. Seismic refraction measurements in the Southern Indian Ocean. *J. Geophys. Res.*, 72: 3015–3042.
- Geller, C.A., Weissel, J.K. and Anderson, R.N., 1983. Heat transfer and intraplate deformation in the central Indian Ocean. *J. Geophys. Res.*, 88: 1018–1032.
- Gutenberg, B. and Richter, C.F., 1954. *Seismicity of the Earth*. Princeton Univ. Press, Princeton, 2nd Edition, 310 pp.
- Johnson, B.D., Powell, C.M. and Veevers, J.J., 1976. Spreading history of the eastern Indian Ocean and greater India's northward flight from Antarctica and Australia. *Geol. Soc. Am. Bull.*, 87: 1560–1566.
- King, G.C.P. and Stein, R.S., 1984. Earthquake potential of active folds. *EOS Trans. Am. Geophys. Union*, 65: 1113 (abstract).
- Laughton, A.S., 1975. General Bathymetric Chart of the Oceans (GEBCO). Canadian Hydrographic Service, Ottawa, Sheet 5.05, 5th ed.
- Liu, C.-S., Sandwell, D.T. and Curray, J.R., 1982. The negative gravity field over the 85°E Ridge. *J. Geophys. Res.*, 87: 7673–7686.
- Liu, C.-S., Curray, J.R. and McDonald, J.M., 1983. New constraints on the tectonic evolution of the eastern Indian Ocean. *Earth Planet. Sci. Lett.*, 65: 331–342.
- Luyendyk, B.P. and Davies, T.A., 1974. Results of DSDP Leg 26 and the geologic history of the southern Indian Ocean. In: *Initial Reports of the Deep Sea Drilling Project*, 26: 909–943.
- McAdoo, D.C. and Sandwell, D.T., 1984. Folding of oceanic lithosphere. *EOS Trans. Am. Geophys. Union*, 65: 1104 (abstract).
- Mutter, J.C. and Cande, S.C., 1983. The early opening between Broken Ridge and Kerguelen Plateau. *Earth Planet. Sci. Lett.*, 65: 369–376.
- Nabelek, J.L., 1984. Determination of earthquake source parameters from inversion of body waves. Ph.D. Thesis, Mass. Inst. of Technol., Cambridge, 342 pp.
- Pearce, J.W., 1978. The northward motion of India since the late Cretaceous. *Geophys. J. R. Astron. Soc.*, 52: 277–311.
- Poppe, B.B., Naab, D.A. and Perry, J.S., 1978. Seismograph station codes and characteristics. U.S. Geol. Surv. Circular 791, 171 pp.
- Raleigh, C.B., Healy, J.H. and Bredehoeft, J.D., 1972. Faulting and crustal stress at Rangely, Colorado. In: H.C. Heard, I.Y. Borg, N.L. Carter and C.B. Raleigh (Editors), *Flow and Fracture of Rocks*. Am. Geophys. Union, Geophys. Monogr. Ser., 16: 275–284.
- Richardson, R.M. and Solomon, S.C., 1977. Apparent stress and stress drop for intraplate earthquakes and tectonic stress in the plates. *Pure Appl. Geophys.*, 115: 317–331.
- Richardson, R.M., Solomon, S.C. and Sleep, N.H., 1979. Tectonic stress in the plates. *Rev. Geophys. Space Phys.*, 17: 981–1019.
- Rothe, J.P., 1969. *The Seismicity of the Earth, 1953–1965*. UNESCO, Paris, 336 pp.
- Rundle, J.B., Kanamori, H. and McNally, K.C., 1984. An inhomogeneous fault model for gaps, asperities, barriers, and seismicity migration. *J. Geophys. Res.*, 89: 10219–10231.
- Schlich, R., 1982. The Indian Ocean: aseismic ridges, spreading centers, and ocean basins. In: A.E.M. Nairn and F.G. Stehli (Editors), *The Ocean Basins and Margins: The Indian Ocean*. Plenum Press, New York, 6: 51–148.
- Sclater, J.G. and Fisher, R.L., 1974. The evolution of the east central Indian Ocean, with emphasis on the tectonic setting of the Ninetyeast Ridge. *Geol. Soc. Am. Bull.*, 85: 683–702.
- Stein, S., 1978. An earthquake swarm on the Chagos-Laccadive Ridge and its tectonic implications. *Geophys. J. R. Astron. Soc.*, 55: 577–588.
- Stein, S. and Okal, E.A., 1978. Seismicity and tectonics of the Ninetyeast Ridge area: evidence for internal deformation of the Indian plate. *J. Geophys. Res.*, 83: 2233–2246.
- Stover, C.W., 1966. Seismicity of the Indian Ocean. *J. Geophys. Res.*, 71: 2575–2581.
- Sykes, L.R., 1970. Seismicity of the Indian Ocean and a possible nascent island arc between Ceylon and Australia. *J. Geophys. Res.*, 75: 5041–5055.
- Sykes, L.R. and Sbar, M.L., 1974. Focal mechanism solutions of intraplate earthquakes and stresses in the lithosphere. In: L. Kristjansson (Editor), *Geodynamics of Iceland and the North Atlantic Area*. D. Reidel, Hingham, pp. 207–224.
- Veevers, J.J., 1977. Models of the evolution of the eastern Indian Ocean. In: J.R. Heirtzler, H.M. Bolli, T.A. Davies, J.B. Saunders and J.G. Sclater (Editors), *Indian Ocean Geology and Biostratigraphy*. Am. Geophys. Union, Washington, pp. 151–163.
- Weissel, J.K., Anderson, R.N. and Geller, C.A., 1980. Deformation of the Indo–Australian plate. *Nature*, 287: 284–291.
- Wiens, D.A. and Stein, S., 1983. Age dependence of oceanic intraplate seismicity and implications for lithospheric evolution. *J. Geophys. Res.*, 88: 6455–6468.
- Zoback, M.L. and Zoback, M., 1980. State of stress in the conterminous United States. *J. Geophys. Res.*, 85: 6113–6156.